

# Ambient RF Energy Harvesting in Urban and Semi-Urban Environments

Manuel Piñuela, *Student Member, IEEE*, Paul D. Mitcheson, *Senior Member, IEEE*, and Stepan Lucyszyn, *Senior Member, IEEE*

**Abstract**—RF harvesting circuits have been demonstrated for more than 50 years, but only a few have been able to harvest energy from freely available ambient (i.e., non-dedicated) RF sources. In this paper, our objectives were to realize harvester operation at typical ambient RF power levels found within urban and semi-urban environments. To explore the potential for ambient RF energy harvesting, a city-wide RF spectral survey was undertaken from outside all of the 270 London Underground stations at street level. Using the results from this survey, four harvesters (comprising antenna, impedance-matching network, rectifier, maximum power point tracking interface, and storage element) were designed to cover four frequency bands from the largest RF contributors (DTV, GSM900, GSM1800, and 3G) within the ultrahigh frequency (0.3–3 GHz) part of the frequency spectrum. Prototypes were designed and fabricated for each band. The overall end-to-end efficiency of the prototypes using realistic input RF power sources is measured; with our first GSM900 prototype giving an efficiency of 40%. Approximately half of the London Underground stations were found to be suitable locations for harvesting ambient RF energy using our four prototypes. Furthermore, multiband array architectures were designed and fabricated to provide a broader freedom of operation. Finally, an output dc power density comparison was made between all the ambient RF energy harvesters, as well as alternative energy harvesting technologies, and for the first time, it is shown that ambient RF harvesting can be competitive with the other technologies.

**Index Terms**—Ambient RF, energy harvesting, maximum power point tracking (MPPT), multiband, rectenna, RF survey, RF-dc.

## I. INTRODUCTION

FOR ALMOST 50 years, far-field RF technology has been used to remotely power systems from relatively large unmanned helicopters [1] to very small smart dust sensors [2] and contact lenses that measure eye pressure [3]. With all these systems, a dedicated RF source is used, where the operator may have control over the effective isotropically radiated power (i.e., both transmit power and antenna characteristics), beam pointing and polarization of the RF source, ensuring optimal line-of-sight operation between the source transmitter (TX) and harvesting receiver (RX). It is important to highlight that this work will

focus only in radiative power transfer and not inductive or near-field power transfer, as demonstrated in [4]. A more convenient solution, however, is to power these devices from ambient RF energy sources, such as television and mobile phone signals, thus removing the need for a dedicated source. As ambient RF levels are lower than those that can be provided by a dedicated RF source, the efficiency of the harvesting system, and its minimum startup power are of critical importance.

In order to assess the feasibility of deploying ambient RF energy harvesters, the available RF power needs to be measured in different locations. Such measurements, in conjunction with knowledge on harvester performance, can then be used to determine the locations at which RF harvester powered devices can be successfully deployed. Several RF spectral surveys, which measure ambient RF power levels from sources such as television and mobile phone base stations, have been previously reported. Many have been undertaken using personal exposimeters or spectrum analyzers, where the exact location of each measurement is unknown and with RF power levels only being reported under general scenarios (e.g., outdoor, indoor, street, bus, etc.) [5], [6]. While being of academic interest for health-related research [7], the lack of power level and specific time/location information limits their usefulness for exploitation in ambient RF energy harvesting applications.

Most rectennas (normally comprising an antenna, impedance matching network, rectifier, storage element, and load) presented in the open literature have been tested using dedicated sources rather than harvesting from ambient RF energy [8]. In recent years, efficiencies as high as 78% [9] and 90% [10] have been demonstrated with relatively high input RF power levels (i.e.,  $> +10$  dBm). Moderate efficiencies have also been achieved using dedicated TXs that provided relatively low input RF power levels; e.g., an efficiency of 60% was achieved with  $-22.6$ -dBm input power [11]. In one demonstrator [12], designed to operate over a broad range of input RF power levels, ( $-30$  to  $+30$  dBm), the efficiency increased from 5% at a low input RF power to a peak of 80% at  $+25$  dBm.

Despite advancements in end-to-end (i.e., input RF to output dc) power conversion efficiencies at low input RF power levels (similar to those measured in the spectral surveys), only a few attempts at true ambient RF energy harvesting have been reported. For example, one relatively efficient rectenna, utilizing a modified omnidirectional patch antenna, has an efficiency of 18% with a single-tone input RF power of  $-20$  dBm [13]. This dedicated signal source was meant to emulate the input RF power levels measured from a nearby digital TV (DTV) TX in Tokyo, Japan, but did not take into account the more realistic effect of harvesting from a modulated broadband signal. Another attempt

Manuscript received November 20, 2012; revised April 24, 2013; accepted April 26, 2013. Date of publication May 24, 2013; date of current version June 28, 2013. This work was supported in part by the U.K. Government and the Mexican National Council of Science and Technology (CONACYT).

The authors are with the Department of Electrical and Electronic Engineering, Imperial College London, London SW7 2AZ, U.K. (e-mail: m.pinuela09@imperial.ac.uk; paul.mitcheson@imperial.ac.uk; s.lucyszyn@imperial.ac.uk).

Color versions of one or more of the figures in this paper are available online at <http://ieeexplore.ieee.org>.

Digital Object Identifier 10.1109/TMTT.2013.2262687

at harvesting ambient RF energy from a mobile phone base station at 845 MHz was reported in [14]. This prototype managed to power an LCD thermometer for 4 min, but only after harvesting for 65 h. In that work, when the authors used a dedicated signal source with a single-tone input RF power of  $-15$  dBm, an efficiency of 3% was recorded. A batteryless location sensor has also been demonstrated [15], powered by a rectenna with a printed antenna on a flexible substrate and a solar cell, although no details for the RF-dc efficiency were reported. Finally, successful prototypes capable of harvesting energy using TV antennas were presented, but again no details of their efficiency were given [16], [17].

In order to demonstrate the feasibility for implementing ambient RF energy harvesting, here we first present the results of a citywide RF spectral survey, indicating suitable locations and associated RF bands with sufficient input RF power density levels for harvesting. Based on these results, rectennas were then fabricated and their efficiencies, under ambient RF energy harvesting operation, were calculated using *in-situ* field strength measurements. Furthermore, an investigation of multiband rectenna arrays is also presented, demonstrating the tradeoffs between series (voltage summing) and parallel (current summing) topologies with the aim of reducing the minimum input power required for harvester operation. Finally, a comparison between measured ambient RF energy harvesting and alternative forms of energy harvesting technologies is presented; highlighting, for the first time, the practical feasibility of exploiting existing freely available sources of RF energy.

## II. LONDON RF SURVEY

In order to quantify input RF power density levels present in a typical urban and semi-urban environment, a citywide RF spectral survey within the ultrahigh frequency (0.3–3 GHz) part of the frequency spectrum was conducted within Greater London. A number of citywide RF spectral surveys have previously been conducted, but in general, only a few samples were taken, giving little insight into (semi-)urban environments [14], [18], [19]. Other surveys [20], [21] compare their measurements relative to the distance from the nearest TX. In a (semi-)urban environment, this may not provide enough information about the RF spectrum since there is likely to be local geographical variations in base-station density and propagation characteristics (e.g., multipath effects and diffraction around and attenuation through buildings).

Each station on the London Underground network was used as a survey point to provide a robust dataset for representing Greater London in terms of geographical distribution and population density, having a combination of urban (in the center) and semi-urban (in surrounding areas) characteristics. Measurements were taken at each of the 270 stations (from a randomly chosen exit, at street level and a height of 1.6 m). To provide traceability and for use as a historical reference, time stamps and GPS locations were recorded. In addition, measurements were taken inside a building at Imperial College London (ICL), to represent a typical office block within an urban environment.

### A. Methodology

Mobile phone usage varies during the daytime, and hence, ambient RF energy in their bands is expected to be time dependant, with more energy available during the daytime than at night time. Therefore, in order to be able to make fair comparisons between locations, measurements were taken between 10:00 am and 3:00 pm on weekdays over a period of one month (between March 5, and April 4, 2012). Electric field strength was measured between 0.3–2.5 GHz using an Agilent N9912A FieldFox RF analyzer [22] with a calibrated Aaronia BicoLOG 20300 omnidirectional antenna [23]. It is important to note that the spectral measurements were undertaken during the analog-to-digital switchover period in the U.K. and so the measurements for DTV may represent an underestimate of present RF power levels measured now that the switch over is complete [24]. It should also be noted that this survey was conducted prior to the 4G network being switched on within the U.K.

A “panning method,” which complies with international regulations for measuring exposure limits, was used [25]–[27]. Here, the calibrated antenna is rotated to three orthogonal axes while the spectrum analyser is set to “max-hold,” ensuring that the maximum reading is recorded. For each measurement, more than 1 min was allocated to allow for more than three sweeps across the selected frequency range. Additionally, to maintain a comparable signal-to-noise (S/N) ratio, attenuation was introduced (with a minimum set at 5 dB) to avoid compression when high input RF power levels were detected. For all measurements, the resolution bandwidth (BW) was fixed at 100 kHz, the internal amplifier was turned on and the highest resolution of 1001 points was selected. These settings provide the ability to obtain a snapshot of the power density that can be expected in an urban or semi-urban environment from continuously variable sources.

### B. Results

After inputting the manufacturers’ frequency-banded antenna factors into the spectrum analyzer, to ensure a fully calibrated system, the electric field strength measurements were taken. The input RF power density ( $S$ ) is then calculated from the electric field strength measurement. Fig. 1 shows the input RF power density measured outside the Northfields London Underground station, where the spectral bands for DTV, GSM900, GSM1800, 3G, and Wi-Fi can be clearly identified.

A well-designed rectenna should ideally be capable of harvesting energy across an entire band, and thus it is important to calculate the total band power. The banded input RF power density  $S_{BA}$  ( $\text{nW}/\text{cm}^2$ ) is calculated by summing all the spectral peaks across the band (i.e., in a similar way, the spectrum analyzer calculates channel power). These levels provide a snapshot of source availability at the time and location of the measurement. Moreover, they are used as a harvester design starting point since the power density at each band will define the input impedance of a rectenna.

The exact frequencies for each band are set by the U.K.’s official frequency band allocation [28]; the GSM900, GSM1800 and 3G base transmit (BTx) bands were separated from the associated mobile transmit (MTx) bands. Table I shows average

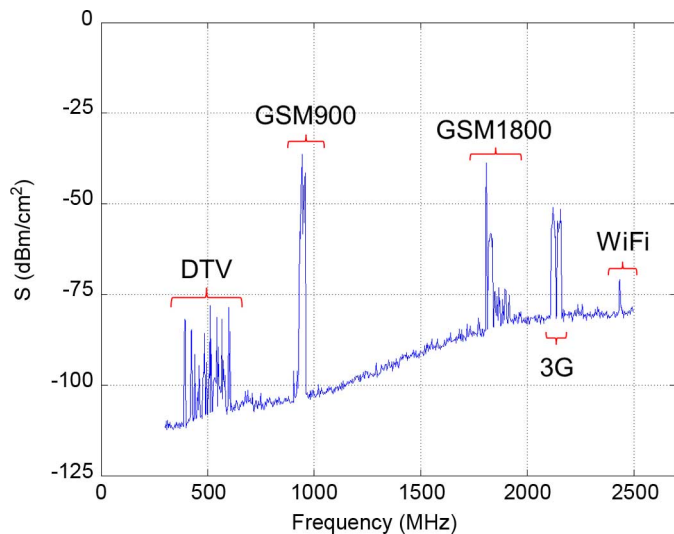


Fig. 1. Input RF power density measurements outside the Northfields London Underground station.

TABLE I  
SUMMARY OF LONDON RF SURVEY MEASUREMENTS

Band	Frequencies (MHz)	Average $S_{BA}$ (nW/cm <sup>2</sup> )	Maximum $S_{BA}$ (nW/cm <sup>2</sup> )
DTV (during switch over)	470-610	0.89	460
GSM900 (MTx)	880-915	0.45	39
GSM900 (BTx)	925-960	36	1,930
GSM1800 (MTx)	1710-1785	0.5	20
GSM1800 (BTx)	1805-1880	84	6,390
3G (MTx)	1920-1980	0.46	66
3G (BTx)	2110-2170	12	240
WiFi	2400-2500	0.18	6

RF power levels across all London Underground stations for the banded input RF power density measurements. It can be seen that all base-station transmit levels are between one and three orders of magnitude greater than the associated MTx levels. For this reason, and the fact that the population of transmitting mobile phones in close proximity of the harvester is highly variable, only base-station TXs will be considered further.

From our London RF survey, DTV, GSM900, GSM1800, 3G, and Wi-Fi were identified as potentially useful ambient RF energy harvesting sources, although DTV appears to be heavily dependent on line-of-sight and sudden changes in atmospheric conditions (e.g., temperature inversion) and Wi-Fi is very dependent on user traffic. It should be noted that the mobile phone base-station TXs employ vertically polarized antennas, placing a constraint on harvester orientation in deployment. With DTV, within the U.K., the main TXs have horizontally polarized antennas, while repeater TXs have vertically polarized antennas.

It is convenient to define the boundary between urban and semi-urban environments by the line that separates zones 3 and 4 on the London Underground map [29]. As one would expect, the central zones 1–3 host the highest density of base stations. As shown in Table II, a banded input RF power density threshold was selected to filter the ten London Underground stations with the highest measurements for each band. With DTV, the highest

TABLE II  
INPUT RF POWER DENSITY THRESHOLD: LONDON UNDERGROUND STATIONS WITHIN CENTRAL ZONES 1–3 (URBAN) AND OUTER ZONES 4–9 (SEMI-URBAN)

Band	$S_{BA}$ Threshold (nW/cm <sup>2</sup> )	Number of Stations	
		Urban	Semi-urban
DTV (during switch over)	40	10	0
GSM900	230	8	2
GSM1800	450	7	3
3G	62	6	4

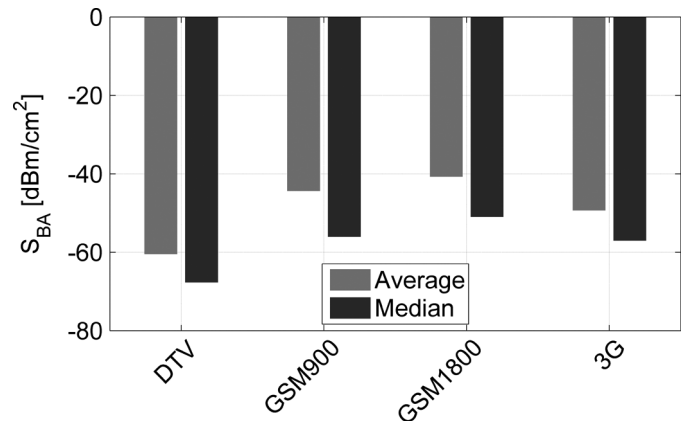


Fig. 2. Banded input RF power density measurements for the four largest ambient sources in Greater London.

recorded measurements were all found within the urban environment. This is because Greater London's main DTV TX (at Crystal Palace) is located on the southeastern border of zones 3 and 4 and there are no London Underground stations further south. With mobile phones, more than 50% of the stations were inside the urban environment and those in a semi-urban environment were all located in close proximity to a cluster of base-station TXs.

Using the complete dataset from the London RF survey, Fig. 2 shows the average and median of the banded input RF power density measurements for the four largest ambient RF sources in Greater London. It can be seen that more than half of the locations have below average power levels. This is due to the fact that several stations had maximum levels that were considerably higher than the average because of their close proximity to TV TXs (e.g., Crystal Palace), extremes in base-station density and propagation characteristics.

In addition to the London RF survey, measurements within the Department of Electrical and Electronic Engineering building at ICL were taken on the 11th floor of the south stairwell. These are shown in Table III. As can be seen, DTV and GSM900 have a higher than average power level, due to a near line of sight from the TV TX and a close proximity to the 2G GSM900/1800 base stations.

The dataset from the London RF survey, with all relevant information (e.g., locations, timestamps, and banded input RF power density measurements), can be found at our interactive website: [www.londonrfsurvey.org](http://www.londonrfsurvey.org) [30]. These measurements were used to design efficient harvesters and compared to ICL

TABLE III  
MEASURED BANDED INPUT RF POWER DENSITIES AT ICL

	DTV	GSM900 (BTx)	GSM1800 (BTx)	3G (BTx)
$S_{BA}$ [ $\text{nW}/\text{cm}^2$ ]	18	48	50	3

measurements to identify locations in Greater London where the designed harvesters could operate. The design procedures and prototype test measurements will be presented in the following sections.

### III. SINGLE-BAND AMBIENT RF ENERGY HARVESTERS

In order to implement efficient ambient RF energy harvesters, designed for the banded input RF power density levels measured at ICL, a set of single-band prototypes were realized and characterized; these will be compared to multiband array architectures in Section V.

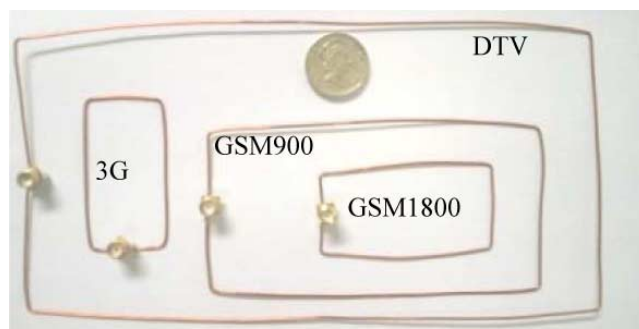
#### A. Antenna Design and Measurements

Since our harvesters are intended to operate within a general (semi-)urban environment, where the exact location of the TX source is unknown, the rectennas' antennas need to be as close to omnidirectional as possible, avoiding the need for beam-pointing during deployment. This is at the obvious expense of limited antenna gain, and therefore, the corresponding levels of  $P_{RF}$  that the rectifier can receive. Conversely, if the location of the TX is known, then it may be tempting to use a high gain antenna, but this would require an appropriate level of beam-pointing and polarization matching that can be established and maintained.

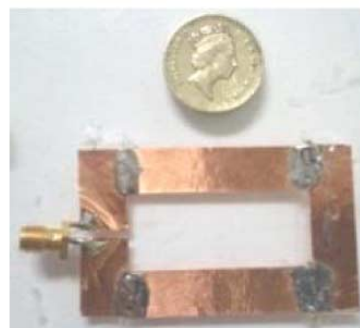
Another requirement is that the antennas need to be easily scalable across all frequency bands since one important objective for this work is to compare and contrast different banded harvesters. Finally, the antennas need to be easily fabricated. For all these reasons, a linear polarized folded dipole was selected, although a monopole would also be suitable [31].

To simplify impedance matching between the antenna and rectifier, a modified folded dipole was used to obtain the required  $50\text{-}\Omega$  reference input impedance. A balun does not need to be employed, as there is no significant degradation in performance for this particular application, even with the use of an unbalanced microstrip rectifying circuit [32]. Furthermore, the antenna was not integrated onto a substrate, to give the additional freedom to embed the harvester on windows or within walls, furnishings, fixtures, or fittings. To this end, two different antennas were fabricated for each band; one made using a  $560\text{-}\mu\text{m}$  diameter copper wire and the other with  $75\text{-}\mu\text{m}$ -thick  $25\text{-mm}$ -wide copper tape. The fabricated antennas are shown in Fig. 3. Since the copper tape was not rigid enough to retain its shape, it was placed on a Perspex substrate, to represent a flat panel.

To design the antennas, full-wave 3-D electromagnetic simulations were performed using CST Microwave Studio. As discussed previously, the antennas were designed to be as omnidirectional as possible, while covering as much of the ambient RF source BW as possible. Fig. 4 shows the typical simulated gain profile for the DTV tape antenna, having a front-to-back ratio



(a)



(b)

Fig. 3.  $50\text{-}\Omega$  folded-dipole antennas shown next to a British £1 coin. (a) DTV, GSM900 (BTx), GSM 1800 (BTx) and 3G (BTx) copper wire antennas. (b) 3G (BTx) copper tape antenna on Perspex.

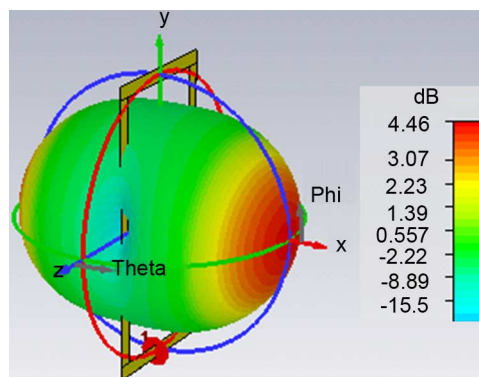


Fig. 4. Simulated beam profile for the DTV tape antenna.

of unity. Table IV shows the simulated gain and the 10-dB return-loss fractional BW for the optimized copper wire and tape antennas.

Fig. 5 shows excellent agreement between predicted and measured return-loss results, within a 10-dB return-loss bandwidth, for the eight fabricated single-band antennas. As one would expect with such a simple classical antenna, the out-of-band performances (not shown) were also in good agreement. It was found that better return-loss measurements are achieved with our single-band antennas when compared to other reported single-band omnidirectional [13] and multiband [33] designs. The latter may be important, as it may be tempting to implement a more compact multiband rectenna, but which

TABLE IV  
SIMULATED GAIN AND 10-dB RETURN LOSS FRACTIONAL BW FOR  
FOLDED-DIPOLE SINGLE-BAND ANTENNAS

Band	Wire		Tape		
	BW (%)	Gain (dBi)	BW (%)	Gain (dBi)	BW (%)
DTV	26	4.35	4	4.48	6
GSM900	3.7	4.42	4.3	4.73	4.3
GSM1800	4.1	4.32	5.3	4.73	10.7
3G	2.8	4.39	5.4	4.76	12

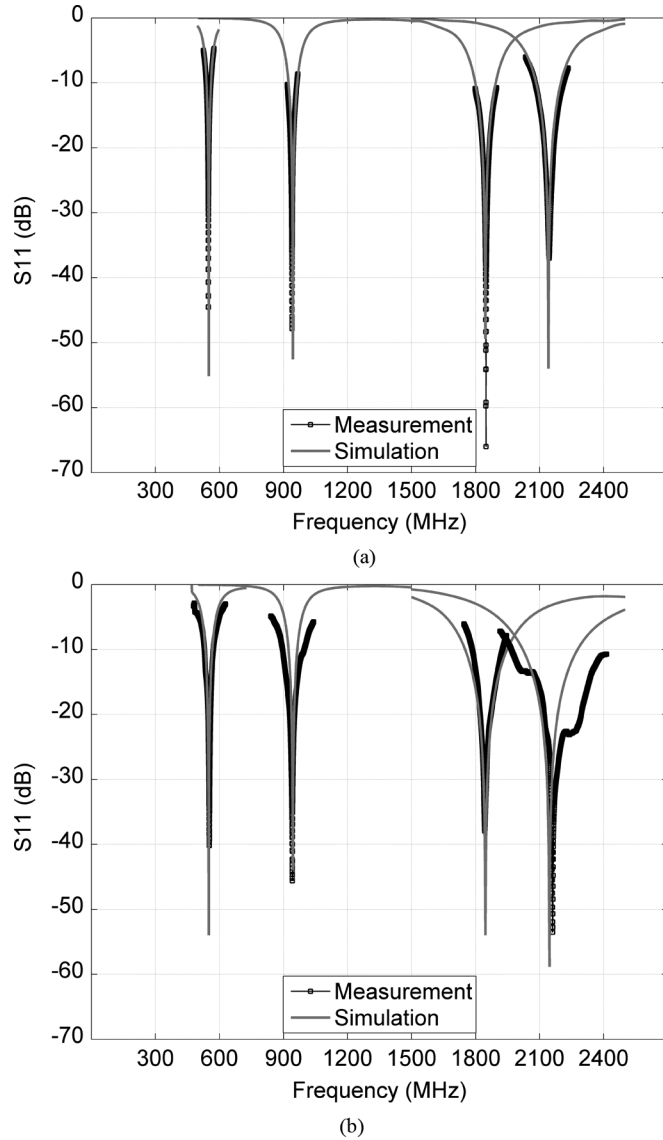


Fig. 5. Input return-loss predictions and measurements for all single-band folded-dipole antennas. (a) Wire. (b) Tape.

may ultimately not give better ambient RF energy harvesting performance.

Obtaining a minimum acceptable return loss over an antenna fractional bandwidth as large as that of the source is key to harvest as much input RF energy as possible. As can be seen in Table IV, where the fractional bandwidth is defined for a 10-dB return loss, our antennas have a fractional bandwidth greater than those of the sources, with the exception of DTV, which

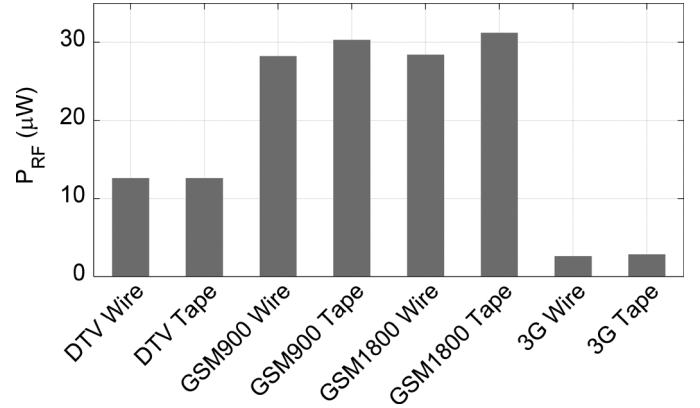


Fig. 6. Predicted input RF power levels for the four largest ambient sources at the ICL testing location.

only covers approximately 35% of the target frequency range. In other work [13], 5-dB return-loss fractional bandwidth is adopted for RF energy harvesting applications.

The fractional bandwidth of the antennas having a minimum return loss of 5 dB is too great to assume a constant antenna gain over the whole band. Therefore, an additional advantage of using 10-dB return-loss fraction bandwidths is that (1) can be used to calculate the input RF power with the assumption that the midband antenna gain is constant with frequency [34]. Therefore, the time-averaged input RF power  $P_{RF}$  is given by

$$P_{RF} = S_{BA} \cdot A_{\text{real}} \text{ and } A_{\text{real}} \approx G(f_o) \frac{\lambda_o^2}{4\pi} \quad (1)$$

where  $A_{\text{real}}$  is the real aperture (or capture area) of the antenna,  $\lambda_o$  is the free-space wavelength at the midband frequency  $f_o$ , and  $G(f_o)$  is the rectenna's antenna gain at  $f_o$ .

Substituting the measured banded input RF power densities recorded in Table III and the predicted midband antenna gains in Table IV into (1), realistic values for  $P_{RF}$  can be calculated for all four bands, with the results shown in Fig. 6. It can be seen that with all antenna gains being in the region of  $\sim 4.5$  dBi, the 2G GSM900/1800 harvesters will generate the highest input RF power levels, due to the high-banded input RF power density levels measured *in situ*. At the other extreme, the 3G harvesters will be the worst performers. As only a small fraction of the required frequency range is covered by the DTV antennas, the predicted values for  $P_{RF}$  represent an overestimation.

### B. Rectifier Design and Measurements

Based on a previously reported analysis [35] and the predicted input RF power levels presented in Fig. 6, the zero-bias SMS7630 diode (in a series configuration) was selected as the optimal solution for our ambient RF energy harvesters, as shown in Fig. 7. In a series configuration, the junction capacitance ( $C_j(V)$ ) of the diode dominates the detector's impedance, as long as  $C_{\text{out}} > C_j(V)$ , and thus  $C_{\text{out}}$  has little or no effect on the matching circuit. This allows  $C_{\text{out}}$  to be large enough to provide a ripple-free output voltage. In contrast,  $C_{\text{out}}$  must be less than 1 pF to achieve a good impedance match with a shunt configuration as  $C_{\text{out}}$  appears in parallel with  $C_j(V)$  and the packaging parasitic capacitance. However,  $C_{\text{out}}$  is too small to

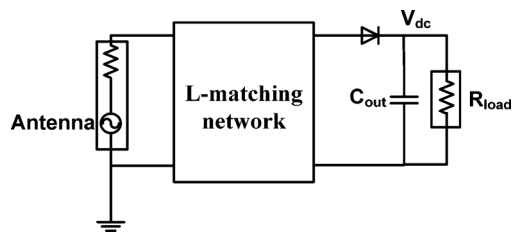


Fig. 7. Series detector configuration with L-matching network.

provide a ripple-free dc voltage to the load. This can be overcome with a matching network that will allow a good impedance match with a large output capacitor, but at the expense of introducing losses. Furthermore, as shown in [36], these issues start to become negligible with a shunt configuration as the shunt diode becomes more self-biased as the input power increases. Simulations were performed using Agilent Technologies' ADS software. Its Momentum package not only takes into account the losses from the low-cost FR4 substrate, but also calculates fringing fields, effects from which are passed on to the harmonic-balance package for simulating the nonlinear behavior of the rectifier.

A good impedance match was achieved by employing a simple matching network; a series lumped-element inductor was used to absorb part of the capacitive reactance from the series diode and an additional quarter-wavelength short-circuit shunt stub was employed to achieve the desired  $50\text{-}\Omega$  impedance [37]. Since the impedance of the diode varies with frequency and input RF power, impedance matching between the antenna and rectifier was first undertaken by finding the optimal output load resistance for an input RF power level of  $-20\text{ dBm}$  with a single-tone source at the midband frequency. After the optimal load was found, further broadband optimization was performed to the matching network and the load to ensure good impedance matching throughout the target frequency range and the measured  $P_{\text{RF}}$  for each band.

As with the antenna analysis, and unlike conventional RF circuits that adopt the more traditional half-power bandwidth definition, the rectifier should adopt the 10-dB-input return-loss bandwidth. The reason for this is that, for ambient RF energy harvesting applications, the input RF power is at a premium and so what little energy is available should not be wasted by being reflected back from avoidable impedance mismatches at either the antenna or rectifier.

Fig. 8 shows excellent agreement between predicted and measured input return loss results, within the  $-10\text{-dB}$  bandwidth, for the DTV and GSM900 rectifiers, having fractional bandwidths of 5.7% (below target) and 4.8%, respectively. With these lower frequency designs, the fundamental and higher order harmonics were below  $-55\text{ dBm}$ , ensuring a clean dc voltage at the load, without the need for any output filtering. Reasonable agreement was found with the GSM1800 and 3G rectifiers, having fractional bandwidths of 1.6% (below target) and 7.4%, respectively. It was found that with these two higher frequency designs, the higher order harmonics were  $-40\text{ dBm}$  at the output. This reduced performance, as illustrated in Fig. 8, is due to the higher series inductive reactance leads of the output shunt storage capacitor. For this reason, a

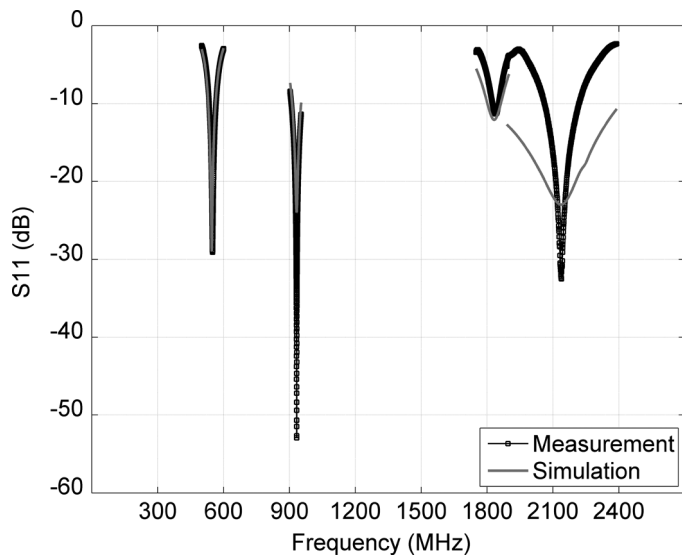


Fig. 8. Input return-loss predictions and measurements for all first prototype single-band rectifiers, with  $P_{\text{RF}} = -20\text{ dBm}$  at the input and optimal load resistances at the output.

second prototype version (v2) was designed for the 3G rectifier, using distributed-element components for the input impedance matching stage and an additional output filter stage. With the lumped-element matching network, it was found that in order to achieve good input impedance matching to  $50\text{ }\Omega$ , all the microstrip transmission lines had to have a characteristic impedance of  $92\text{ }\Omega$ . With the distributed-element matching network, a simple shunt quarter-wavelength open-circuit stub, designed for operation at the fundamental frequency, was employed. A microstrip line was added between the cathode of the diode and the stub to absorb the capacitive reactance of the diode. The stub effectively filters to  $< -50\text{ dBm}$  the higher order harmonics. The microstrip design can be seen in Fig. 13.

### C. PMM

Since the input RF power from ambient sources can be represented as a multi-tone source, with power levels fluctuating across the target frequency range, the output impedance of the rectifier is time varying. A power management module (PMM) capable of performing maximum power point tracking (MPPT) is required.

For our work, a low-power integrated-circuit PMM from Texas Instruments Incorporated (BQ25504) was selected, due to its low quiescent current ( $< 330\text{ nA}$ ) and low input voltage operation ( $\sim 80\text{ mV}$  hot-start and  $330\text{-mV}$  cold-start) [38]. It is worth noting that its startup voltage is lower than PMMs previously reported and realized using hybrid circuits for RF energy harvesting [13]. The BQ25504 PMM includes a boost converter that steps up its input voltage (having a  $350\text{-mV}$  average value during ambient operation) to useful levels between  $2.4\text{--}5.3\text{ V}$ . The BQ25504 also has a built-in battery management module, which is used to control the duty cycle of the output power to the load.

MPPT operation on the BQ25504 is achieved by periodically sampling the open-circuit voltage (OCV) at the input of the converter, which then draws a current causing the converter

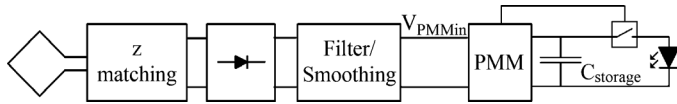


Fig. 9. System block diagram.

input voltage to fall and be held at a pre-programmed fraction of the OCV (set by a potential divider). In a simple dc circuit, with a resistive source impedance, the optimal ratio is 0.5. For the rectenna-based system, a ratio of 0.48–0.53 was found to maximize the power output of the system. The BQ25504 is designed to charge a storage element, and in this case, a capacitor  $C_{\text{storage}}$  was used. The programmed PMM continuously charges the storage capacitor, and the load (a low-power LED) was automatically connected to the storage capacitor when the capacitor voltage reaches an upper limit  $V_{\text{high}} = 2.84$  V and automatically disconnected when it reaches a lower limit  $V_{\text{low}} = 2.40$  V. The duty cycle of the LED can then be used to calculate the efficiency of the system, as will now be described. A diagram of the system is shown in Fig. 9.

#### IV. END-TO-END EFFICIENCY ANALYSIS

The efficiency  $\eta$  of an RF energy harvesting system is

$$\eta = \frac{P_{\text{dc}}}{P_{\text{RF}}} \quad (2)$$

where  $P_{\text{dc}}$  is the time-averaged output (i.e., equivalent dc) power into the storage element (e.g., battery or supercapacitor) and load and  $P_{\text{RF}}$  is as previously defined. Measurements for this type of system are usually performed in a controlled environment (e.g., an anechoic chamber or TEM cell), using a dedicated constant or variable amplitude single-tone RF signal source [32], [39]. However, the former is not suitable for evaluating ambient RF energy harvesting operation, which has a much broader spectrum of nonconstant input frequencies and where the instantaneous input RF power is time variant. The use of a constant single-tone dedicated source provides a convenient stable reference power to the harvester; while the latter reflects a more realistic signal source having fluctuating power levels across a nonzero bandwidth, multipath, and reflection effects which are very difficult to emulate in a controlled environment.

Therefore, to determine the overall end-to-end efficiency  $\eta_{\text{e-e}}$  for a complete ambient RF energy harvester, the input RF energy  $U_{\text{RF}}$  was calculated based on the harvester's antenna characteristics and the actual banded input RF power density measurements taken at the time of harvester operation, using the Agilent Fieldfox and the calibrated antenna. It is important to note that since the impedance mismatch between the antenna and detector is not taken into account,  $U_{\text{RF}}$  is higher than expected, providing an underestimate of end-to-end efficiency. The output dc energy  $U_{\text{dc}}$  was then calculated by measuring the charge–discharge cycle time,  $t_{\text{cycle}}$  of the storage capacitor between  $V_{\text{high}}$  and  $V_{\text{low}}$ , as the LED is repeatedly connected and disconnected. The output dc energy equation is already taking into account the efficiency of the PMM given the fact that the measurements

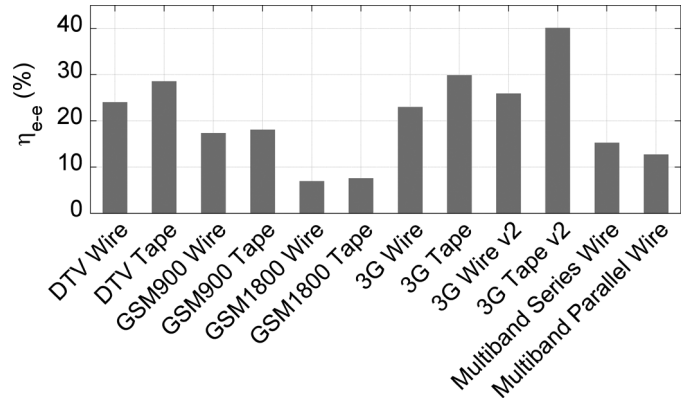


Fig. 10. End-to-end efficiencies for ambient RF energy harvesting at ICL.

are taken at its output voltage. The end-to-end efficiency of one charge–discharge cycle of  $C_{\text{storage}}$  is

$$\eta_{\text{e-e}} = \frac{U_{\text{dc}}}{U_{\text{RF}}} \quad (3)$$

where the input RF energy is given by integrating the time-averaged input RF power over a cycle time, as

$$U_{\text{RF}} = \int_0^{t_{\text{cycle}}} P_{\text{RF}} dt \quad (4)$$

and the output dc energy is given by the energy supplied to the load, as follows:

$$U_{\text{dc}} = C_{\text{storage}} \frac{(V_{\text{high}}^2 - V_{\text{low}}^2)}{2}. \quad (5)$$

##### A. ICL Field Trials

Four single-band ambient RF energy harvesters were assembled by connecting the rectifiers to the wire/tape antennas and PMMs programmed for the optimal load. A 100- $\mu\text{F}$  shunt capacitor was employed as the storage element, providing  $U_{\text{dc}} = 115$   $\mu\text{J}$ . Our system is capable of cold-starting the boost converter and MPPT since the rectenna is capable of providing the minimum starting voltage of 330 mV. When the minimum voltage is reached, the boost converter and MPPT start to operate and the charge–discharge cycle at the load begins, causing the LED to flash. During field trials,  $t_{\text{cycle}}$  took up to 170 s for the harvester with lowest banded input RF power density, corresponding to 3G with the wire antenna. Table V summarizes the results where  $t_c$  and  $t_d$  are the charge and discharge times, respectively, and  $\Sigma V$  and  $\Sigma I$  are the multiband voltage and current summing array architectures, respectively. A detailed discussion on the multiband rectenna arrays will be presented in the following section. The end-to-end efficiency was calculated using (3) with data from Fig. 6 and measuring the charge–discharge cycle time during harvesting operation.

Fig. 10 shows the overall end-to-end efficiencies for all the harvester demonstrators, deployed and tested at ICL. As predicted by simulations, the improved 3G v2 demonstrator with

TABLE V  
HARVESTERS CHARGE AND DISCHARGE TIMES ( $t_c$ ,  $t_d$ , RESPECTIVELY) FOR A SPECIFIED LOAD

Band	Wire					Tape				
	$t_c$ (s) load independent	$t_d$ (s) load dependant	$t_{cycle}$ (s) load dependant	$P_{dc}(t_d)$ ( $\mu$ W)	$P_{dc}(t_{cycle})$ ( $\mu$ W)	$t_c$ (s) load independent	$t_d$ (s) load dependant	$t_{cycle}$ (s) load dependant	$P_{dc}(t_d)$ ( $\mu$ W)	$P_{dc}(t_{cycle})$ ( $\mu$ W)
DTV	26	12	38	9.6	3	14	18	32	8.2	3.6
GSM900	14	10	24	11.5	4.8	8	13	21	14.4	5.5
GSM1800	43	15	58	7.7	2	22	27	49	5.2	2.4
3G v2	167	3	170	38.4	0.7	96	5	101	1.2	1.1
Multiband $\Sigma$ V	43	7	50	66	2.3	-	-	-	-	-
Multiband $\Sigma$ I	55	5	60	92.2	2	-	-	-	-	-

tape antenna outperformed its original design by 11%; achieving an end-to-end efficiency of 40% with an input RF power of only  $-25.4$  dBm.

It is believed that a much greater efficiency can be achieved for the DTV harvester if the fractional bandwidths for the first prototype circuits (i.e., 4.4/4.5% for the antennas and 5.8% for the rectifier) could be increased to match the much greater target value of 26%. Likewise, the reduced efficiency of the GSM1800 harvesters can be attributed to the detrimental effects of the narrowband input impedance matching of the rectifier (i.e., having a fractional bandwidth of only 1.6%, when compared to its target value of 4.1%). Finally, with all the harvesters, the end-to-end efficiencies can be enhanced through better antenna design and optimal polarization matching.

Table VI, shows the number of locations from the London RF survey that would be able to support our harvesters. Unlike the single-band 3G harvester, which can operate at 45% of the locations, our DTV harvester can only be used at two locations (one in zone 2 and the other in zone 3). Therefore, for the general deployment of an ambient RF energy harvester within an (semi-)urban environment, at street level, the single-band DTV harvester may not be practical

## V. ARRAY ARCHITECTURES

Since ambient input RF power levels can be low (i.e., below  $-25$  dBm) and dependent on both time and spatial considerations, harvesters could be designed to extract energy with spatial-diversity within the same frequency band or using different frequency bands. For example, with the former, at a particular location there may be only one band that has significant levels of RF energy worth harvesting. In this case, spatial-diversity array architectures may provide more usable output power. Alternatively, with the latter, multiband array architectures may provide more robust operation.

With both forms of parallel array architecture (i.e., spatial-diversity and multiband), a further classification can be seen through the use of either diversity/band switching or a summing node. With the former, physical switches automatically select whichever signal path delivers the highest input RF power level;

TABLE VI  
NUMBER OF LOCATIONS FROM THE LONDON RF SURVEY CAPABLE OF SUPPORTING IDENTICAL HARVESTERS AT THE SAME EFFICIENCY LEVELS

	DTV	GSM900 (BTx)	GSM1800 (BTx)	3G (BTx)
Stations with higher $S_{BA}$	2	28	68	122

with the latter, power from all signals is combined. Fig. 11 illustrates generic forms of parallel array architectures, showing that switching/summing can be performed electromagnetically at a single antenna or at the output from multiple antennas, rectifiers, or PMMs.

Multiband array architectures, similar to those in Fig. 11(c) and (d), capable of RF harvesting from the four previously identified bands, were selected as possible optimal solutions, given no size/cost constraints. Our objectives were to reach the minimum cold-start voltage at the lowest possible input RF power levels and increase the harvesters' operational capabilities within (semi-)urban environments.

To this end, two different multiple rectenna architectures were investigated. The first with a single shared PMM and the second with multiple PMMs, as illustrated in Fig. 12. To simplify assembly, the wire antennas were selected since they did not require a substrate. Unwanted coupling between the single-band antennas was minimized by placing them a minimum distance of  $\lambda_L/5$  apart; where  $\lambda_L$  is the wavelength of the lowest frequency band antenna [40]. For example, the DTV and the 3G antennas were kept at least 11 cm apart, as shown in Fig. 13. This allowed  $S_{11}$  measurements to be the same as in Fig. 5 once all antennas were assembled into the array.

### A. Multiple Rectennas With a Shared PMM

In order to improve the cold-start performance of the system, the outputs of multiple rectennas can be connected in series, as shown in Fig. 12(a). This increases the probability of the voltage on the input of the PMM reaching the cold-start level (330 mV for the BQ25504) under any given scenario. While cold-starting the PMM, each rectenna harvests (albeit not optimally). Once

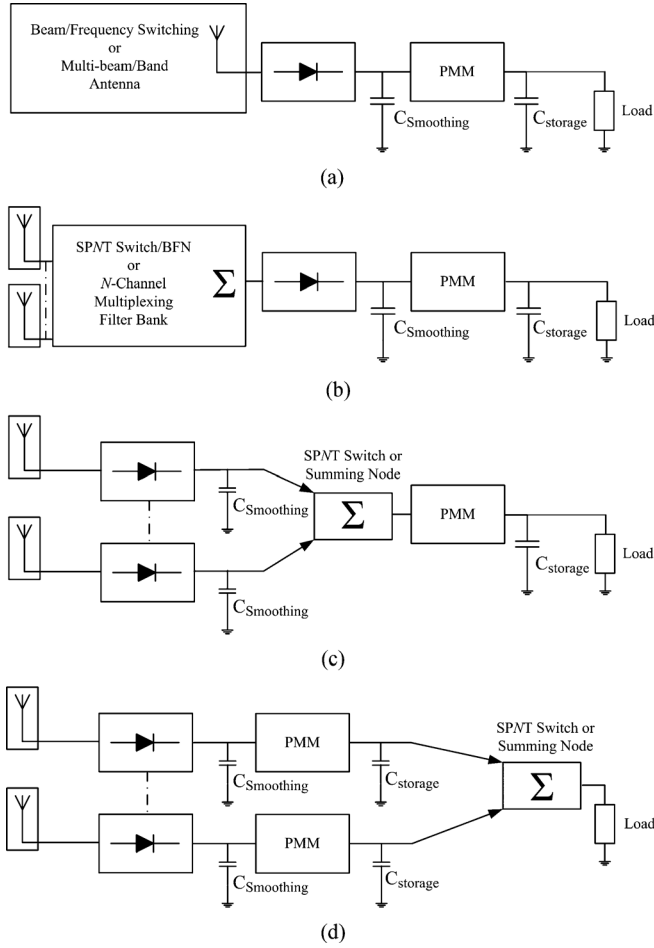


Fig. 11. Parallel array architectures with switching/summing at the: (a) antenna, (b) output of multiple PMMs, (c) output of multiple rectifiers, and (d) output of multiple PMMs.

the PMM circuit starts, with the MPPT operating, the harvested power level increases.

The behavior of the series rectenna topology with a shared PMM requires some discussion. As the output impedance and the OCV for each rectenna is different, since they operate at different frequencies and input RF power levels, the rectennas are forced to share the same output current in a series configuration, which does not allow them all to operate at their individual maximum power points. This causes the voltage on each rectenna output, except the one having the highest input RF power, to collapse. This operation is analogous to the partial shading problem with a series string of solar panels [41] sharing a common boost converter. With this photovoltaic system, bypass diodes placed around individual cells stop the poorly lit cells contributing a negative voltage (and power) to the string. In our case, the series circuit formed by the loop antennas and rectifying diodes performs the same task. This means that while all rectennas contribute to system startup, only the rectenna with the highest input RF power contributes significant power for continuous operation once the PMM starts. Fig. 10 shows the end-to-end efficiency for the voltage summing multiband harvester array when tested at ICL. An efficiency of only 15% was achieved with a

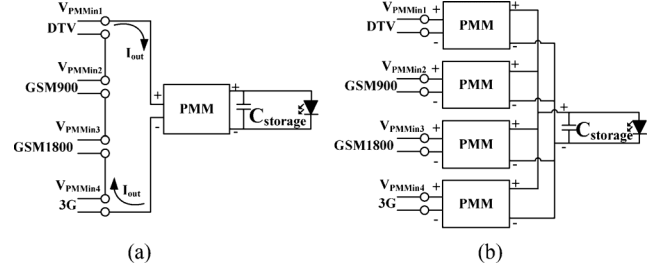


Fig. 12. Multiband array architectures (with  $N = 4$  bands). (a) Voltage summing at the outputs of the single-band rectennas. (b) Current summing at the outputs of the single-band harvesters.

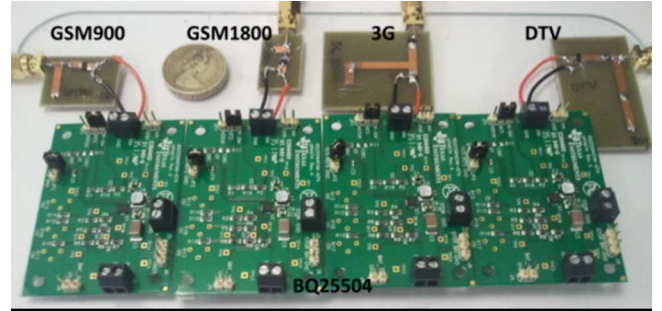


Fig. 13. Rectenna array architecture with individual PMMs for the four largest contributors with wire antennas.

combined input RF power of  $-12$  dBm. The lower efficiency, when compared to a single-band harvester, is due to the imbalance of rectifier outputs, as discussed above. Here, the charge time was 43 s, compared to 167 s with the lowest contributing single-band 3G harvester with wire antenna.

### B. Multiple Rectennas With Individual PMMs

In order to overcome the balancing issues when multiple rectennas share a common PMM, as discussed previously, each rectenna can have its own PMM, whose outputs can be connected to a common storage element (in this case, a  $400\text{-}\mu\text{F}$  shunt capacitor, providing  $U_{\text{dc}} = 461\ \mu\text{J}$ ), as illustrated in Fig. 12(b) and shown in Fig. 13. Although not achieving cold-start as quickly as the series topology, this parallel topology has the advantage of being able to run each rectenna at its maximum power point. In addition, once one rectenna is able to harvest enough energy for a cold-start, all PMMs will start because they share a common storage element, allowing the rectennas with low-input RF power levels to harvest at levels below which they could not do so independently.

This parallel topology was tested and found to be capable of operating in many locations where the series array was unable to operate; e.g., if only one of the bands had  $P_{\text{in}} > -25$  dBm. As expected, the largest contributor hot-started the other PMMs, allowing them to harvest at an input RF power level down to  $-29$  dBm.

However, as with the previous results for voltage summing, having a combined input RF power of  $-12$  dBm, the efficiency using multiple PMMs is slightly lower, at 13%, as shown in Fig. 10. This is because useful dc output power from the cold-

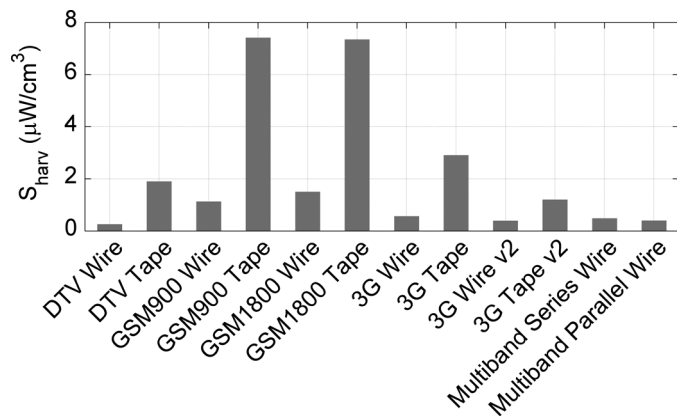


Fig. 14. Output dc power density for all harvesters at ICL.

starting harvester is being supplied to the other harvesters for hot-starting, even though some of them may not actually be contributing any of their own harvested power.

## VI. OUTPUT DC POWER DENSITY COMPARISON

The volumetric output dc power density  $S_{\text{harv}}$  ( $\mu\text{W}/\text{cm}^3$ ) represents an important figure of merit for comparing alternative energy harvesting technologies. For ambient RF energy harvesting, the output dc power is calculated by multiplying the effective input RF power by the overall end-to-end-efficiency. The total volume (including that of the antenna, rectifier, and PMM; not including energy storage, as this does not directly affect the dc power output) must be determined. It is important to note that the volume for the antenna could effectively disappear if it is assembled onto a window or within a wall, furnishing, fixture, or fitting. Moreover, the required PMM printed circuit board (PCB) size used throughout these calculations was assumed to be ten times the size of the BQ25504 chip, to account for any necessary additional components.

Fig. 14 shows the output dc power density for all the harvesters demonstrated here. It can be seen that the 2G GSM900/1800 harvesters with tape antennas both have the highest value of  $S_{\text{harv}} = 7.4$  ( $\mu\text{W}/\text{cm}^3$ ), when tested at ICL, due to the high-banded input RF power density  $S_{BA}$ . The value for the most efficient harvester (i.e., 3G v2 with tape antenna) was not the highest in terms of output RF power because  $S_{BA}$  in this band was more than an order of magnitude lower than with GSM900.

$S_{\text{harv}}$  allows a direct and meaningful comparison to be made with other alternative energy harvesting technologies. Our best performing ambient RF energy harvester (i.e., GSM900 with tape antenna) was compared against alternative energy harvesting technologies, assuming they used the same PMM board size [42]–[44].

It can be seen in Fig. 15 that ambient RF energy harvesting has a low output dc power density when compared to alternative energy harvesting technologies, but only when the total volume of the first prototype demonstrator is considered. However, when the antenna is absorbed onto or into a background

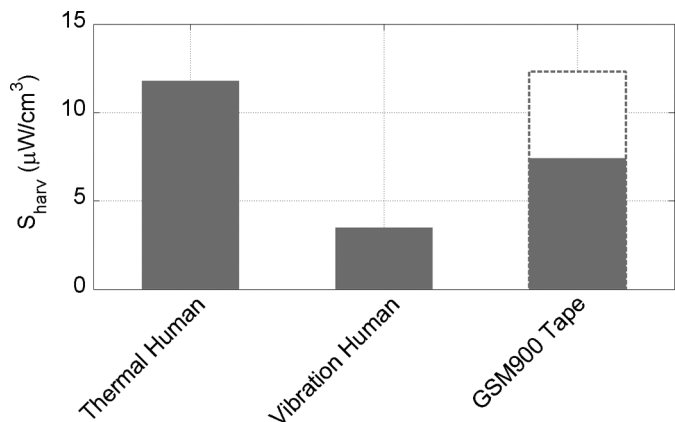


Fig. 15. Output dc power density comparison for alternative ambient harvesting technologies [40]–[43] against the best current generation of RF harvesters at ICL.

feature and when the PMM is fully integrated into the rectifier, it can outperform (as indicated by the dotted column) the alternative energy harvesting technologies, while providing a complimentary means of extracting energy from the environment. The RF harvesters, however, have the additional advantage in that they do not require a thermal gradient, and unlike vibration-driven devices, they have no moving parts.

## VII. CONCLUSIONS

Our objectives were to reach the lowest possible ambient input RF power levels and extend the harvesters' operational capabilities within (semi-)urban environments. To this end, a comprehensive citywide RF spectral survey was undertaken, indicating that more than 50% of the 270 London Underground stations are suitable locations for the deployment of our ambient RF energy harvesters. It has been demonstrated that single-band harvesters can operate with efficiencies of up to 40% in a (semi-)urban environment, and can start to operate from power levels as low as  $-25$  dBm.

To increase the freedom of operation, multiband array architectures were investigated. With the current summing harvester arrays, RF harvesting was achieved at an input RF power level as low as  $-29$  dBm, without any external dc power supply to hot-start the PMM. Limitations on the multiband array architectures were discussed, highlighting the need for further work in balancing rectennas with voltage summing rectenna arrays when operating at lower input RF power levels.

Finally an output dc power density comparison against alternative energy harvesting technologies has shown that RF harvesting can represent a competitive solution within (semi-)urban environments, especially when the antenna can be absorbed into background features.

## ACKNOWLEDGMENT

The authors would like to thank the members of the London RF survey team and F. Kusidlo, Agilent EEsof EDA, for his advice regarding simulations.

## REFERENCES

- [1] “Demonstration of microwave power transmission,” *Pract. Wireless*, pp. 835–835, 1965.
- [2] T. Salter, G. Metzke, and N. Goldsman, “Parasitic aware optimization of an RF power scavenging circuit with applications to smartdust sensor networks,” in *IEEE Radio Wireless Symp.*, 2009, pp. 332–335.
- [3] “SENSIMED Triggerfish®—Continuous IOP monitoring,” SENSIMED, Lausanne, Switzerland, Mar. 2012. [Online]. Available: <http://www.sensimed.com/S-Trig-glaucoma.htm>, “
- [4] M. Piñuela, D. C. Yates, S. Lucyszyn, and P. D. Mitcheson, “Maximizing DC-to-load efficiency for inductive power transfer,” *IEEE Trans. Power Electron.*, vol. 28, no. 5, pp. 2437–2447, May 2013.
- [5] W. Joseph, G. Vermeeren, L. Verloock, M. M. Heredia, and L. Martens, “Characterization of personal RF electromagnetic field exposure and actual absorption for the general public,” *Health Phys.*, vol. 95, no. 3, pp. 317–330, Sep. 2008.
- [6] G. Thuroczy, F. Molnar, J. Szabo, G. Janossy, N. Nagy, G. Kubinyi, and J. Bakos, “Public exposure to RF from installed sources: Site measurements and personal exposimetry,” in *1st Eur. Antennas Propag. Conf.*, 2006, pp. 1–4.
- [7] P. Elliott, M. B. Toledano, J. Bennett, L. Beale, K. de Hoogh, N. Best, and D. J. Briggs, “Mobile phone base stations and early childhood cancers: Case-control study,” *Br. Med. J.*, vol. 340, no. 1, pp. 1–7, Jun. 2010.
- [8] N. Shinohara, “Power without wires,” *IEEE Microw. Mag.*, vol. 12, no. 7, pp. S64–S73, Dec. 2011.
- [9] J. Y. Park, S. M. Han, and T. Itoh, “A rectenna design with harmonic-rejecting circular-sector antenna,” *IEEE Antennas Wireless Propag. Lett.*, vol. 3, pp. 52–54, 2004.
- [10] “Dengyo rectennas,” Nihon Dengyo Kosaku Company Ltd., Tokyo, Japan, Jul. 2012. [Online]. Available: <http://www.den-gyo.com/solution/solution01.html>
- [11] T. Le, K. Mayaram, and T. Fiez, “Efficient far-field radio frequency energy harvesting for passively powered sensor networks,” *IEEE J. Solid-State Circuits*, vol. 43, no. 5, pp. 1287–1302, May 2008.
- [12] V. Marian, B. Allard, C. Vollaïre, and J. Verdier, “Strategy for microwave energy harvesting from ambient field or a feeding source,” *IEEE Trans. Power Electron.*, vol. 27, no. 11, pp. 4481–4491, Nov. 2012.
- [13] C. Mikeka, H. Arai, A. Georgiadis, and A. Collado, “Dtv band micropower RF energy-harvesting circuit architecture and performance analysis,” in *IEEE Int. RFID-Technol. Appl. Conf.*, 2011, pp. 561–567.
- [14] S. Kitazawa, H. Ban, and K. Kobayashi, “Energy harvesting from ambient RF sources,” in *IEEE MTT-S Int. Microw. Symp. Workshop*, 2012, pp. 39–42, Series on Innovative Wireless Power Transmission: Technol., Syst., Appl.
- [15] R. Vyas, V. Lakafosis, and M. Tentzeris, “Wireless remote localization system utilizing ambient RF/solar power scavenging RFID tags,” in *IEEE MTT-S Int. Microw. Symp. Dig.*, May 23–28, 2010, pp. 1764–1767.
- [16] H. Nishimoto, Y. Kawahara, and T. Asami, “Prototype implementation of ambient RF energy harvesting wireless sensor networks,” *IEEE Sens. J.*, pp. 1282–1287, Nov. 2010.
- [17] A. Sample and J. R. Smith, “Experimental results with two wireless power transfer systems,” in *IEEE Radio Wireless Symp.*, 2009, pp. 16–18.
- [18] V. Nitu, G. Lojewski, and S. Nitu, “Electromagnetic field evaluation on an antennas shared site, EUROCON 2009,” in *IEEE EUROCON’09*, 2009, pp. 70–75.
- [19] Y. Kawahara, K. Tsukada, and T. Asami, “Feasibility and potential application of power scavenging from environmental RF signals,” in *IEEE AP-S Int. Symp.*, 2009, pp. 1–4.
- [20] H. J. Visser, A. C. F. Reniers, and J. A. C. Theeuwes, “Ambient RF energy scavenging: GSM and WLAN power density measurements,” in *38th Eur. Microw. Conf.*, 2008, pp. 721–724.
- [21] T. G. Cooper, S. M. Mann, M. Khalid, and R. P. Blackwell, “Public exposure to radio waves near GSM microcell and picocell base stations,” *J. Radiol. Protection*, vol. 26, no. 2, pp. 199–211, 2006.
- [22] “FieldFox RF Analyser N9912A 4/6 GHz,” Agilent Technol., Santa Clara, CA, USA, Tech. Overview, 2012.
- [23] “Biconical EMC broadband antennas—BicoLOG Series,” Aaronia, Strickscheid, Germany, Data Sheet, 2012.
- [24] “Digital TV switchover in the UK,” Digital UK Ltd., London, U.K., 2012.
- [25] “International commission on non-ionizing radiation protection, guidelines for limiting exposure to time-varying electric, magnetic, and electromagnetic fields (up to 300 GHz),” *Health Phys.*, vol. 74, no. 4, pp. 494–522, 1998.
- [26] M. Riederer, “EMF exposure due to GSM base stations: measurements and limits,” in *IEEE Int. Electromagn. Compat. Symp.*, 2003, vol. 1, pp. 402–405.
- [27] “Revised ECC recommendation (02)04: Measuring non-ionising electromagnetic radiation (9 kHz–300 GHz),” ECC within the Eur. CEPT, Oct. 2003.
- [28] Nat. Freq. Planning Group, “United Kingdom frequency allocation table, issue no. 16,” 2010, Cabinet Official Committee on U.K. Spectrum Strategy.
- [29] Transport for London, “London underground map,” Aug. 2012. [Online]. Available: <http://www.tfl.gov.uk/gettingaround/1106.aspx>
- [30] Imperial College London, “London RF Survey,” Aug. 2012. [Online]. Available: <http://londonrfsurvey.org/>
- [31] R. Vyas, V. Lakafosis, M. Tentzeris, H. Nishimoto, and Y. Kawahara, “A battery-less, wireless mote for scavenging wireless power at UHF (470–570 MHz) frequencies,” in *IEEE AP-S Int. Symp./USNC/URSI Nat. Radio Sci. Meeting*, Jul. 3–8, 2011, pp. 1069–72.
- [32] T. Ugan and L. M. Reindl, “Harvesting low ambient RF-sources for autonomous measurement systems,” in *Proc. IEEE Instrum. Meas. Technol. Conf.*, 2008, pp. 62–65.
- [33] A. Costanzo, A. Romani, D. Masotti, N. Arbizzani, and V. Rizzoli, “RF/baseband co-design of switching receivers for multiband microwave energy harvesting,” *Sensors Actuators A, Phys.*, vol. 179, pp. 158–168, Jun. 2012.
- [34] J. L. Volakis, *Antenna Engineering Handbook*. New York, NY, USA: McGraw-Hill, 2007.
- [35] M. Piñuela, P. D. Mitcheson, and S. Lucyszyn, “Analysis of scalable rectenna configurations for harvesting high frequency ambient radiation,” in *Proc. Power MEMS*, Leuven, Belgium, 2010, pp. 41–44.
- [36] J. O. McSpadden, L. Fan, and K. Chang, “Design and experiments of a high-conversion-efficiency 5.8-GHz rectenna,” *IEEE Trans. Microw. Theory Techn.*, vol. 46, no. 12, pp. 2053–2060, Dec. 1998.
- [37] “HSMS-285x series datasheet,” Avago Technol., San Jose, CA, USA, 2009.
- [38] “Ultra low power boost converter with battery management for energy harvester applications,” Texas Instruments Incorporated, Dallas, TX, USA, BQ25540 Datasheet, 2011.
- [39] A. Nimo, D. Grgic, and L. M. Reindl, “Ambient electromagnetic wireless energy harvesting using multiband planar antenna,” in *IEEE 9th Int. Syst., Signals, Devices Multi-Conf.*, Mar. 20–23, 2012, pp. 1, 6.
- [40] H. Takhedmit, L. Cirio, B. Merabet, B. Allard, F. Costa, C. Vollaïre, and O. Picon, “A 2.45-GHz dual-diode rectenna and rectenna arrays for wireless remote supply applications,” *Int. J. Microw. Wireless Technol.*, vol. 3, no. 3, pp. 251–258, Jun. 2011.
- [41] S. Vemuru, P. Singh, and M. Niamat, “Modeling impact of bypass diodes on photovoltaic cell performance under partial shading,” in *IEEE Int. Electro/Information Technol. Conf.*, 2012, pp. 1–5.
- [42] P. D. Mitcheson, E. M. Yeatman, G. K. Rao, A. S. Holmes, and T. C. Green, “Energy harvesting from human and machine motion for wireless electronic devices,” *Proc. IEEE*, vol. 96, no. 9, pp. 1457–1486, Sep. 2008.
- [43] R. J. M. Vullers, R. V. Schaijk, H. J. Visser, J. Penders, and C. V. Hoof, “Energy harvesting for autonomous wireless sensor networks,” *IEEE Solid-State Circuits Mag.*, vol. 2, no. 2, pp. 29–38, Spring, 2010.
- [44] V. Leonov, P. Fiorini, S. Sedky, T. Torfs, and C. Van Hoof, “Thermoelectric MEMS generators as a power supply for a body area network,” in *13th Int. Solid-State Sens., Actuators, Microsyst. Conf. Tech. Dig.*, vol. 1, pp. 291–294.



**Manuel Piñuela** (M’12) received the BSc. degree in electrical and electronic engineering from the National Autonomous University of Mexico (UNAM), Mexico City, Mexico, in 2007, and is currently working toward the Ph.D. degree at Imperial College London, London, U.K.

From 2006 to 2009, he worked in industry as an Electronic Design and Project Engineer for companies focused on oil and gas services in both Mexico and the US. His research interests are wireless power transfer, RF power amplifiers, and

RF energy harvesting.

Mr. Piñuela was the recipient of the Gabino Barrera Medal.



**Paul D. Mitcheson** (SM'12) received the M.Eng. degree in electrical and electronic engineering and Ph.D. degree from Imperial College London, U.K., in 2001 and 2005, respectively.

He is currently a Senior Lecturer with the Control and Power Research Group, Electrical and Electronic Engineering Department, Imperial College London. His research interests are energy harvesting, power electronics, and wireless power transfer. He is involved with providing power to applications in circumstances where batteries and cables are not

suitable. His work has been sponsored by the European Commission, EPSRC and several companies.

Dr. Mitcheson is a fellow of the Higher Education Academy.



**Stepan Lucyszyn** (M'91–SM'04) received the Ph.D. degree in electronic engineering from King's College London (University of London), London, U.K., in 1992, and the D.Sc. (higher doctorate) degree from Imperial College London, London, U.K., in 2010.

He is currently a Reader (Associate Professor) of millimeter-wave electronics and Director of the Centre for Terahertz Science and Engineering, Imperial College London. After working in industry as a Satellite Systems Engineer for maritime and military communications, he spent the first 12 years researching microwave and millimeter-wave RF integrated circuits (RFICs)/monolithic microwave integrated circuits (MMICs), followed by RF microelectromechanical systems (MEMS) technologies. He has coauthored approximately 140 papers and 11 book chapters in applied physics and electronic engineering. He has delivered many invited presentations at international conferences.

Dr. Lucyszyn was an associate editor for the *JOURNAL OF MICROELECTROMECHANICAL SYSTEMS* (2005–2009). In 2011, he was the chairman of the 41st European Microwave Conference, Manchester, U.K. In 2005, he was elected Fellow of the Institution of Electrical Engineers (IEE), U.K., and Fellow of the Institute of Physics, U.K. In 2008, was invited as a Fellow of the Electromagnetics Academy, USA. In 2009, he became an IEEE Distinguished Microwave Lecturer (2010–2012). He is currently an Emeritus DML for 2013 and a newly appointed European Microwave Lecturer (EML) for the European Microwave Association.